

Study on pyrite thermoelectricity, ore-forming fluids and H-O-Rb-Sr isotopes of the Yongxin gold deposit, Central Asian Orogenic Belt: Implications for ore genesis and exploration

Cheng-Lu Li^{a,b}, Lin Li^{c,d,*}, Mao-Wen Yuan^{b,c}, Masroor Alam^e, Sheng-Rong Li^{b,c}, M. Santosh^{b,f}, Chang-zhou Deng^g, Hao Liu^{b,c}, Guo-Zhan Xu^a

^a Heilongjiang Institute of Geological Survey, Harbin, Heilongjiang 150036, China

^b School of Earth Science and Resources, China University of Geosciences, Beijing 100083, China

^c State Key Laboratory of Geological Processes and Mineral Resources, China University of Geosciences, Beijing 100083, China

^d Institute of Earth Sciences, China University of Geosciences, Beijing 100083, China

^e Department of Earth Sciences, Karakoram International University, Gilgit 15100, Pakistan

^f Centre for Tectonics, Resources and Exploration, Dept. of Earth Sciences, University of Adelaide, SA 5005, Australia

^g Key Laboratory of Ore Deposit Geochemistry, Institute of Geochemistry, Chinese Academy of Sciences, Guiyang 550081, China

ARTICLE INFO

Keywords:

Pyrite thermoelectricity
Fluid inclusion
H-O-Rb-Sr isotope
Mineralogical mapping
Central Asian Orogenic Belt

ABSTRACT

The Yongxin gold deposit is one of the prominent gold deposits in the Duobaoshan gold-copper metallogenic belt within the eastern domain of the Central Asian Orogenic Belt. The deposit has recently been discovered therefore, its genesis and economic significance remain unknown. Here, we present the results of pyrite thermoelectricity, fluid inclusion and H-O-Rb-Sr isotopic studies of different minerals with a view to decipher ore genesis and ore prospecting in the Yongxin gold deposit. The Rb-Sr isotopic composition of pyrite, quartz and calcite indicate that the deposit was formed at 114.6 ± 1.2 Ma. Fluid inclusions and H-O isotopic studies show that the Yongxin gold deposit was formed at shallow depth, with relatively low ore-forming temperatures (120–355 °C), low-medium salinity (0 wt% to 10 wt%), and low-moderate density (0.6–1.0 g/cm³). The ore-forming fluids were mainly magmatic which mixed with meteoric water triggering the precipitation of ore-forming materials. We trace the evolution of the ore fluids from deeper levels in the northwest part of the deposit to shallower levels in the southeast. The thermoelectricity parameter values (X_{np}) of pyrite range from -188 to -85 and the values of erosional or exhumation level (γ) range from 97% to 71% with an average of 79.4%, suggesting that the existing ore-body is the lower part of the deposit (79.4% of the ore-body has already been eroded). Thermoelectricity of pyrite shows a vertical distribution in the axial direction without significant change in the X_{np} values, indicating that the ore body extends further. Combined with the pyrite thermoelectric coefficients in different altitudes, we predict gold potential for the ores at further depth depending on the continued presence of the N-P type pyrite. Our mineralogical mappings also suggest a prospecting potential in the two zones at depth beneath the northwestern part of the deposit.

1. Introduction

The Yongxin gold deposit is a fracture-controlled large epithermal gold deposit, located in the southern part of the Duobaoshan gold-copper metallogenic belt within the eastern domain of the Central Asian Orogenic belt (CAOB) (Li et al., 2018a; Yuan et al., 2018; Zhao et al., 2019a; Song et al., 2019). Based on the work of Li et al. (2017a), the U-Pb geochronology of the wall-rocks of the Yongxin gold deposit shows Early Cretaceous ages (113.7 ± 1.8 – 114.8 ± 1.9 Ma) and the

mineralization was related to the magmatic activity. Pyrite, galena, sphalerite, chalcocopyrite, electrum, native gold and tellurides are the major metallic minerals in the Yongxin gold deposit. Most of the gold is found in pyrite suggesting co-precipitation.

Auriferous pyrite in ore deposits has been taken as a potential proxy for genetic modeling and prospecting of gold deposits (Li et al., 2018a; Li et al., 2019a; Yuan et al., 2017; Yuan et al., 2018). Numerous studies on the thermoelectric properties of pyrite have shown that pyrite is good indicator of mineral composition and crystal structure (Popova,

* Corresponding author at: State Key Laboratory of Geological Processes and Mineral Resources, China University of Geosciences, Beijing 100083, China.
E-mail address: clark.li@cugb.edu.cn (L. Li).

1974; Seifullip, 1978; Chen et al., 1987; Shao et al., 1990; Abratis et al., 2004; Shen et al., 2013; Wang et al., 2016; Wu et al., 2019; Lehner et al., 2007). Pyrite thermoelectric data can be used to constrain the mechanisms of ore-forming condition including temperature, formed depth, deposit scale and ore denudation degree, which are all crucial factors for prospecting (Yang et al., 1999; Li, 1994; Li et al., 2009; Xue et al., 2014; Niu et al., 2016; Alam et al., 2019), and also pyrite thermoelectric technique has been successfully applied in the prospecting and evaluation of some of the world-class gold deposits in the Jiaodong Peninsula in the eastern part of the North China Craton, such as the Sanshandao, Jiaojia, Linglong, Qixia, and Jinqingding gold deposits (Chen et al., 1996; Yang et al., 2000; Shen et al., 2013; Xue et al., 2014). Since the deposit is recently discovered and there are very limited studies carried out on this deposit, and there is completely lack of information on the age of the gold mineralization, the physico-chemical conditions and source of the ore-forming fluids in the Yongxin gold deposit.

This paper presents a detailed report based on pyrite thermoelectricity, fluid inclusion and H-O-Rb-Sr data of different minerals with an aim of establishing ore genesis mechanism, nature, evolution and temperature of ore forming fluids, mineralisation age, current denudation level and future prospecting guidelines in the Yongxin gold deposit. Our study has strong implications for prospecting, ore genesis and exploration of such type of the gold deposits regionally as well globally.

2. Regional geology

The Duobaoshan gold-copper metallogenic belt along the southeastern margin of the Xing'an Block, is the most important metal producing region in the eastern part of the CAOB, which is composed of the Ergun, Xing'an, Songnen and Jiamusi Blocks (Wu et al., 2015) (Fig. 1a). The metal deposits in the Duobaoshan gold-copper metallogenic belt are generally classified as the epithermal-, skarn- and porphyry type. Although different types of deposits have different modes of occurrence and ore textures, and most of these are in the fault-controlled zone. In addition, the metal deposits in the Duobaoshan gold-copper metallogenic belt show a consistent spatial-temporal association with Ordovician and Cretaceous magmatism (Liu et al., 2017; Li, 2018). Several Au-Ag-Cu-Pb-Zn deposits (Paleozoic to Mesozoic) were discovered in the area, including the NW-trending Duobaoshan Cu (Zeng et al., 2014; Zhao et al., 2019b), Tongshan Cu (Hao et al., 2015; Liu et al., 2017), Zhengguang Au (Gao et al., 2017a; Song et al., 2019), Erdaokan Ag-Pb-Zn deposits (Yuan et al., 2019) and NE-trending Sandaowanzi Au (Liu et al., 2013a), Beidagou Au (Gao et al., 2017b), Shangmachang Au (Gao et al., 2018), and Mengdehe Au and Keluo Au deposits (Li, 2018).

Multiple faults control ore concentration in the Duobaoshan gold-copper metallogenic belt, which are closely linked to the Phanerozoic tectonic evolution of the region (Yuan et al., 2018; Gao et al., 2017a; Zeng et al., 2014). The closure of the Paleo-Asian Mongol-Okhotsk Ocean and subduction of the Pacific Plate constructed the regional structural framework of the Eastern part of the CAOB (Deng et al., 2019; Gao et al., 2017b; Zhao and Zhang, 1997; Du et al., 1988).

The lithostratigraphic units in the Duobaoshan gold-copper metallogenic belt are mainly Ordovician Tongshan Formation and Duobaoshan Formation, Silurian-Devonian Niquhe Formation, Cretaceous Longjiang Formation and Guanghua Formation (Yuan et al., 2018; Liu et al., 2017). The Tongshan and Duobaoshan Formations (strike 175–310° and dip 25–30°) are composed of terrigenous clastic rocks and andesite, basalt andesite, rhyolite (Du et al., 1988; Liu et al., 2017). The Silurian-Devonian Formation consists of terrestrial clastic rocks, sandstone, silty sandstone, slate, andesite, basalt andesite, tuff lava and spilite with lenses of limestone. The Cretaceous Longjiang and Guanghua Formations are dominantly composed of andesite, rhyolite, volcanic breccia and tuffs (Yuan et al., 2018; Liu et al., 2017) (Fig. 1b). The intrusive rocks in the region are composed of the Ordovician monzodiorite, Carboniferous granite and granodiorite, Jurassic

granodiorite and monzonitic and Cretaceous alkali feldspar granite and diorite. The volcanic rocks are mainly intermediate and felsic and generally calc-alkaline. The basement is composed of metamorphic rocks (Yuan et al., 2018) (Fig. 1b).

3. Ore deposit characteristics

The Yongxin gold deposit is located in the southern part of the Doubaoshan gold-copper metallogenic belt, in the Huolongmeng village of the Nenjiang County in the Heilongjiang province, Northeast China. It was identified as a large epithermal gold deposit (Yuan et al., 2018; Li, 2018). The alteration and mineralization occurred synchronous with the shallow-level emplacement of dioritic porphyry in the deposit (Li et al., 2017a; Li et al., 2018a; Yuan et al., 2017; Yuan et al., 2018). > 10 ore-body veins have been discovered within the fracture zones and the proved gold reserves are about 21 t. The ore bodies extend for about 1.6 km beneath the surface with a maximum thickness of 73.4 m and highest grade of gold 14.25 g/t. The ore bodies in the Yongxin gold deposit are considered to be genetically related to the NE-trending and NW-trending fault (Li, 2018).

The hydrothermal alteration types of the Yongxin gold deposit mainly include silicification, sericitization and potassic alteration which display successive zoning surrounding the ore-bodies. Among these, silicification is the most important alteration type for the mineralization. Quartz and minor pyrite are the main alteration minerals associated with silicification, and the presences of these minerals is used as a criteria for prospecting in the Yongxin gold deposit. The sericitization zone contains comparatively lesser gold mineralization, characterized by muscovite, chlorite and kaolinite assemblage and overprints on the silicification zone. The potassic alteration occurring on the outermost part of ore bodies is covered by the sericitization. The alteration mineral assemblages include K-feldspar and minor amount of quartz.

Based on the observation of the ore samples and the cross-cutting relationship of the ore minerals, the ore-forming process is divided into following stages: 1) pyrite-quartz stage; 2) pyrite stage; 3) gold-telluride-pyrite-galena-sphalerite stage; 4) carbonate stage. The pyrite-quartz stage is characterized as deficient metal concentration stage. The quartz veins are almost barren with galena, sphalerite and chalcopyrite (Fig. 2a–c). The pyrite stage is composed of numerous pyrite veins in which anhedral and cubic shape pyrite grains are associated with gold (Fig. 3d–f). The gold-telluride-pyrite-galena-sphalerite stage is the main metallogenic stage in terms of gold precipitation, and is associated with various cogenetic tellurides in smoky grey quartz vein (Fig. 3g, h). The carbonate stage belongs to the late metallogenic period, and occurs only along the periphery of the orebody. The carbonate veins cut the different quartz veins of earlier stages (Fig. 3i).

The ore type of the Yongxin gold deposit is mainly hydrothermal cemented tectonic breccia and the surface outcrop of breccia is intensively oxidized displaying maroon color (Fig. 4a). The angular blocks in the breccia are formed of granite. (Fig. 4b). The pyrite occurs as cubes as well as pyritohedron mostly anhedral with porous appearance (Fig. 4c–f), and formed during all the ore-forming stages. The pyrite shows cross-cutting relationship with the galena and sphalerite (Fig. 4g). The chalcopyrite was mainly observed as tiny dots (1–10 μm) in the sphalerite that indicate the co-precipitation with sphalerite and subsequent exsolution (Fig. 4h). Gold is occurred as inclusions in the pyrite, filling fissures and interstitial space between the quartz crystals (Fig. 4i, j). The telluride minerals occur as irregular granular or elongated inclusions in the pyrite grains, and the quartz veins fill fractures in pyrite (Fig. 4k, l). The telluride minerals mainly include hessite, petzite, altaite and tetradyrite, among which hessite is predominant and cogenetic with gold.

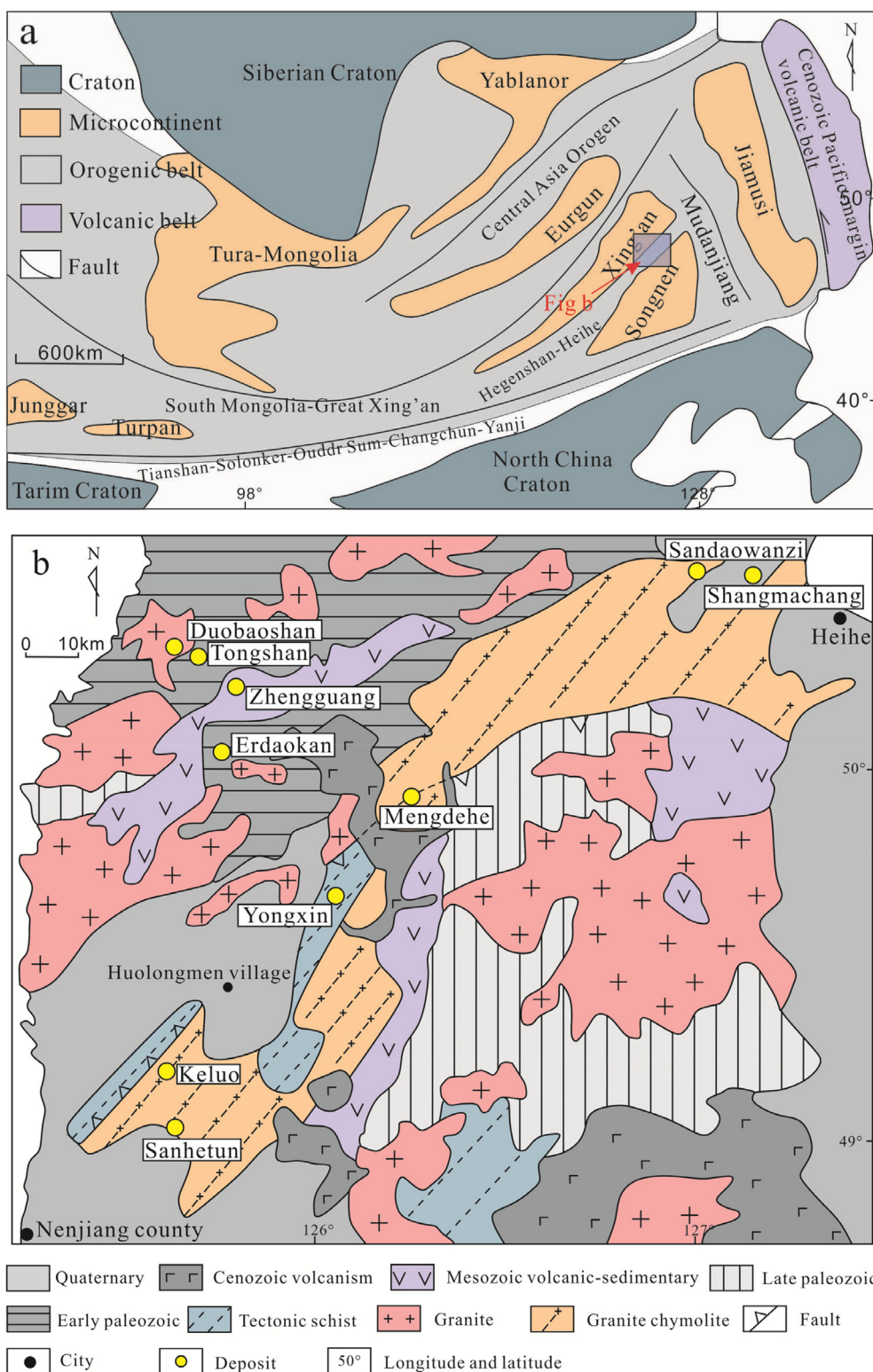


Fig 1. (a) Generalized tectonic framework of the eastern domain of the Central Asian Orogenic Belt, modified after Ge et al. (2007). (b) Simplified geological map of the study area (mainly the Duobaoshan gold-copper metallogenic belt) (modified after Miao et al., 2003; Yuan et al., 2018).

4. Sampling and methodology

4.1. Sampling

A total of 32 representative ore samples were collected from different drill cores for thermoelectric studies, (Fig. 2a). All the samples were crushed to separate the pyrite grains with size of approximately

40–60 mesh. They were ultrasonically cleaned in alcohol and then handpicked to a purity of > 99% under a binocular microscope.

A total of 25 polished thin sections representing different ore forming stages, and 13 polished blocks were prepared for fluid inclusion, ore microscopy and petrographic studies. In addition, 7 quartz samples from different altitude, different exploration lines and different ore forming stages were selected for H-O isotopic analysis. Eight

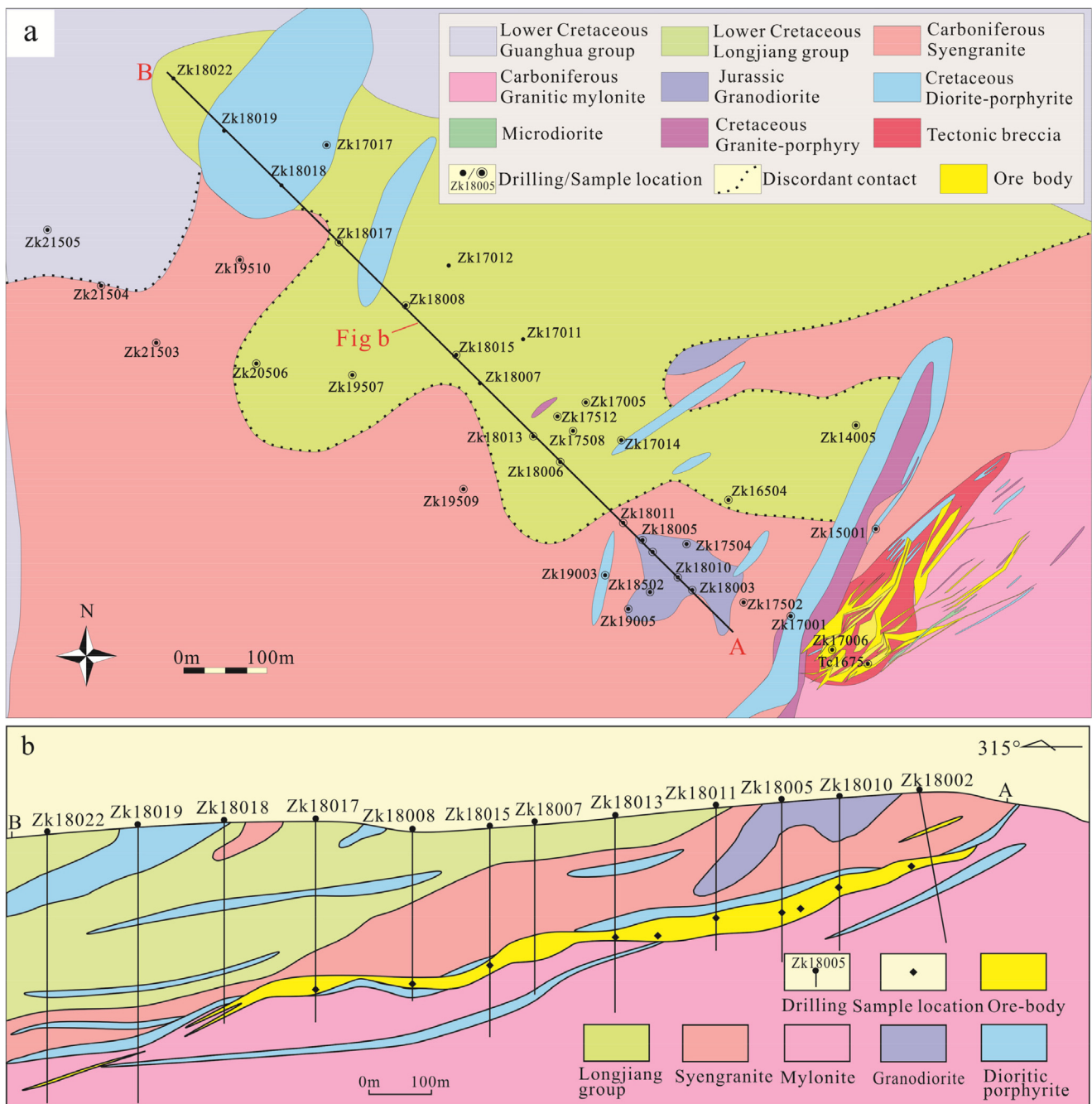


Fig 2. Geological sketch and prospecting line profile map of the Yongxin gold deposit: (a) geological sketch map with the sample locations; (b) No.180 prospecting line profile map (modified after Yuan et al.,2018).

samples (6 pyrite, one quartz and one calcite) were selected from ore-bodies for Rb-Sr isotopic analysis.

4.2. Methodology

4.2.1. Thermoelectricity

As a semiconductor mineral, pyrite shows characteristic electrical properties (Pridmore & Shuey, 1976; Schieck et al.,1990; Abraitis et al., 2004; Savage et al., 2008). The non-equilibrium carriers in pyrite grains diffuse from high-temperature side to low-temperature side, which result in the generation of a thermal electromotive force(± E). This thermoelectric phenomenon is related to the chemical composition of the semiconductor minerals, and is known as the Seebeck effect. In order to quantify this phenomenon, the concept of thermoelectricity

coefficient(α) was proposed, which is defined as (Shao et al.,1990; Wang et al., 2016):

$$\alpha = \frac{\pm E}{t_H - t_C}, [\pm\mu V/^{\circ}C]$$

α: thermoelectricity coefficient, t_H: the hot-end temperature, t_C: the cold-end temperature, ± E: the positive and negative thermal electromotive force (Shao et al., 1990).

The conduction type of the carriers (the positive or negative properties), correlated to the thermal electromotive force (± E) are classified as electronic type (N-type) and hole type (P-type). P-type carriers show positive properties and N-type gives negative. The isomorphous impurities in the composition of pyrite, defects in crystal structure, density, temperature and pressure gradients can affect the

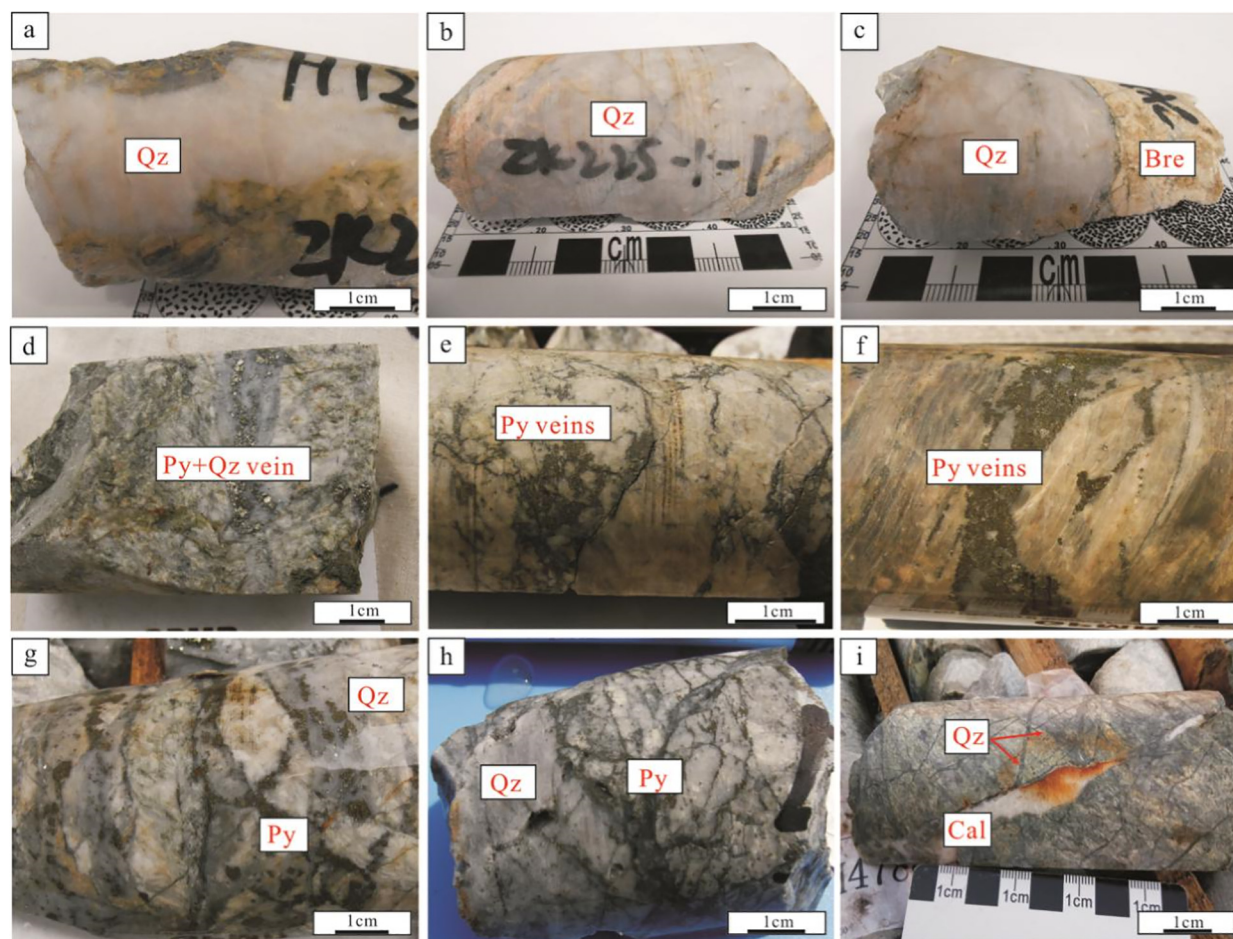


Fig 3. Representative samples of the different mineralization stages. (a)–(c) pyrite-quartz stage; (d)–(f) pyrite stage; (g), (h) gold-telluride-pyrite-galena-sphalerite stage; (i) carbonate stage.

thermoelectricity coefficient of pyrite and the conduction type (Lehner et al., 2007). Therefore, thermoelectricity of pyrite can be used to evaluate the ore-forming conditions, such as temperature, pressure and depth (Abraitis et al., 2004; Shen et al., 2013; Zhang, 2010; Wang et al., 2016; Liu et al., 2018; Alam et al., 2019).

Thermoelectricity of pyrite associated with different drill cores of the Yongxin gold deposit (32 samples and 100 pyrite grains of each sample) was measured by the BHTE-06 thermoelectricity coefficient apparatus with the activation temperature 68 ± 3 °C and ambient temperature 21 °C at the Mineral Typomorphism Laboratory in China University of Geosciences (Beijing). The apparatus was manufactured by Beijing University of Aeronautics and Astronautics (Niu et al., 2016; Alam et al., 2019).

4.2.2. Fluid inclusion microthermometry and H-O-Rb-Sr isotope

Microthermometric measurements were carried out at China University of Geosciences, Beijing, using a Linkam THMSG 600 heating-freezing stage mounted on a ZEISS microscope. The standard measurement temperature was set from -60 °C to 400 °C and the estimated accuracies of the freezing and heating measurements were ± 0.1 °C (from -60 °C to 25 °C), ± 1 °C (from 25 °C to 300 °C), and ± 2 °C (above 300 °C) (Roedder, 1984; Liu and Duan, 1987; Shepherd et al., 1985; Liu, 2001; Lu et al., 2004).

The H-O isotope analyses were performed at the Beijing Research Institute of Uranium Geology (BRIUG), using a DeltaV advantage stable isotope ratio mass spectrometer coupled with a TM-SPCL MIR10 infrared laser. The accuracy of the O isotope analysis is better than $\pm 0.2\%$, and that of the H isotope analysis is better than $\pm 2\%$. Seven

different quartz samples from early to middle stage in the Yongxin gold deposit were analyzed for oxygen and hydrogen isotopic composition.

The isotopic ratios are reported in standard δ notation (‰) relative to SMOW. The Rb-Sr content was analyzed on a VG 354 mass spectrometer at the Center of Modern Analysis, Nanjing University. Reproducibility and accuracy of Sr isotope runs have been periodically checked by running the Standard Reference Material NBS 987 and Laboratory Standard La Jolla, with a mean $^{87}\text{Sr}/^{86}\text{Sr}$ value of 0.710342 ± 0.00040 (certified value: 0.710340 ± 0.000260) and a mean $^{143}\text{Nd}/^{144}\text{Nd}$ value of 0.511840 ± 0.000008 . Data regression and calculation of Rb-Sr isochron ages were determined using Ludwig's Isoplot Program (Ludwig, 2001, 2003), using errors of 1% for $^{87}\text{Rb}/^{86}\text{Sr}$ ratios.

5. Results

5.1. Thermoelectricity

5.1.1. Pyrite thermoelectric coefficients in different altitude

Thermoelectric measurements were conducted on 3200 grains of pyrite separated from 32 drill cores from different altitudes (100–300 m) of the Yongxin gold deposit. The minimum and maximum values of measured thermoelectric coefficients (α) were -306 and 296 $\mu\text{V}/^\circ\text{C}$ respectively, which indicate that the pyrite is either N- (99%) or P-type 1%. Most of the pyrite is N-type in the Yongxin gold deposit. The α values of P-type pyrite range from 5 to 296 $\mu\text{V}/^\circ\text{C}$ whereas the N-type pyrites have α values ranging from -8 to -306 $\mu\text{V}/^\circ\text{C}$ (Table 1).

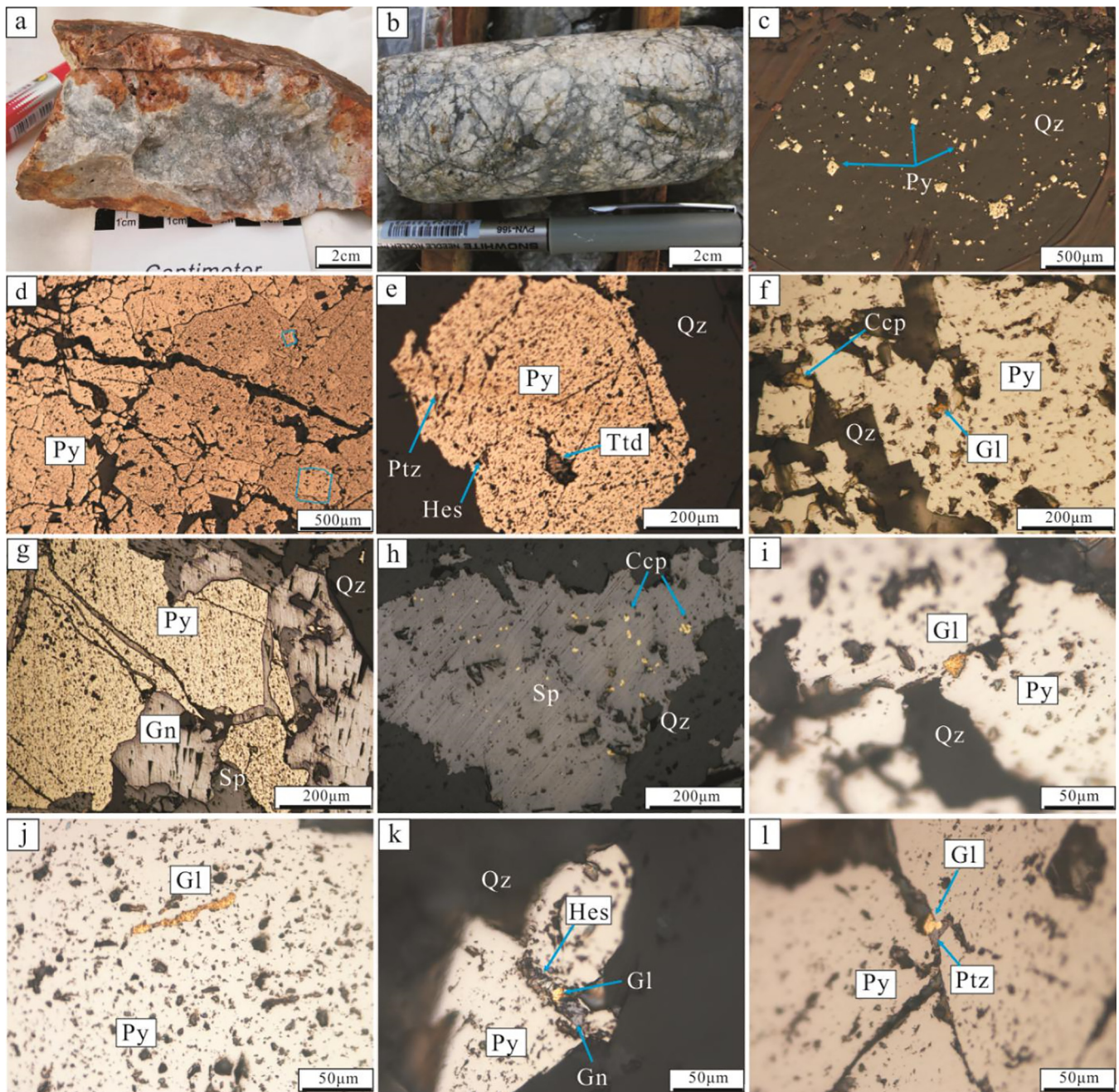


Fig 4. Ore samples and mineral assemblage under microscope. (a) Surface oxidized ore; (b) typical hydrothermal cemented structural breccia ore, (c)–(f) different types of pyrite in the different ore-forming stages; (g) galena and sphalerite occurring in the fissure of pyrite grains; (h) solid solution of chalcopyrite in sphalerite grains; (i) crack-gold in pyrite; (j) inclusion gold in the pyrite; (k) hessite, gold and galena in the pyrite, (l) gold and prytzite occurring in the fissure of pyrite grains.

The zonal distribution of pyrite from bottom to top of the deposit shows that N-type dominates in the deepest level, whereas P-type is abundant in the shallow level, as also reported in previous studies from other deposits (e.g. Karpov, 1981; Large et al., 2009; Shen et al., 2013). The zonal distribution generally follows P-type (shallow section) → P-type + N-type (central section) → N-type (deep section) (Chen et al., 1989; Shao et al., 1990). It can be deduced from Fig. 5 that the pyrite type of the Yongxin gold deposit is mainly N-type, which indicates that it is mainly P-type + N-type zone (central section) from the shallower levels to the deeper levels. From the surface to the 300 m level (altitude), pyrite thermoelectricity coefficient ranges from -285 to $264 \mu\text{V}/^\circ\text{C}$ and, from 300 m level to 200 m level of the orebody, it ranges from -306 to $296 \mu\text{V}/^\circ\text{C}$ while it shows a range between -301 and $286 \mu\text{V}/^\circ\text{C}$ at an altitude from 200 m to 100 m. The negative values

of the thermoelectric coefficient occur below the level of 100 m and range between -252 and $-96 \mu\text{V}/^\circ\text{C}$ (Table 1).

5.1.2. Thermoelectric parameter (X_{np}) of pyrite and ore denudation degree estimation

The pyrite thermoelectric parameter (X_{np}) is related to the erosional or exhumation level of gold deposits, and is calculated by the thermoelectricity coefficient (α). The formula is: $X_{np} = (2f_i + f_{ii}) - (f_{iv} + 2f_v)$, where f corresponds to levels of thermoelectric coefficients of pyrite in the samples, while f_i is $\alpha > 400 \mu\text{V}/^\circ\text{C}$, f_{ii} is α ranging from 200 to $400 \mu\text{V}/^\circ\text{C}$, f_{iii} is α ranging from 0 to $200 \mu\text{V}/^\circ\text{C}$, f_{iv} is α ranging from 0 to $-200 \mu\text{V}/^\circ\text{C}$ and f_v is $\alpha < -200 \mu\text{V}/^\circ\text{C}$ (Yang and Zhang, 1991; Yang and Meng, 1991; Shen et al., 2013; Xue et al., 2014; Wang et al., 2016; Alam et al., 2019). The erosional or exhumation level (γ)

Table 1
The thermoelectric coefficient and other parameters of pyrite in the Yongxin gold deposit.

Altitude range(m)	Drills No. (ZK)	Altitude (m)	N-type (α)			T(°C)	N(%)	P-type (α)			T(°C)	P (%)	Ore-forming Temperature (°C)	Xnp	γ	Average Au grade (ppm)	
			Max	Min	Ave			Max	Min	Ave							
< 100	21,505	40	-130	-252	-182	288	100	\	\	\	\	\	288	-120	80%	1.74	
	21,504	62	-100	-234	-169	294	100	\	\	\	\	\	294	-107	76%	1.44	
	17,017	76	-105	-240	-163	298	100	\	\	\	\	\	298	-109	77%	<1	
	21,503	100	-96	-247	-171	294	100	\	\	\	\	\	294	-118	79%	2.32	
100-200	19,510	110	-60	-278	-159	300	98	248	38	143	159	2	230	-119	80%	1.45	
	20,506	120	-108	-284	-197	279	98	86	76	81	122	2	200	-140	85%	1.18	
	18,017	130	-119	-241	-181	288	100	\	\	\	\	\	288	-115	79%	3.66	
	18,008	140	-53	-226	-151	304	100	\	\	\	\	\	304	-102	75%	1.24	
	19,507	144	-90	-277	-175	291	100	\	\	\	\	\	291	-117	79%	1.00	
	18,015	155	-111	-283	-190	283	99	286	286	286	245	1	264	-130	82%	5.26	
	15,001	180	-53	-232	-131	316	99	148	148	148	162	1	239	-99	75%	<1	
	17,512	187	-39	-244	-169	294	100	\	\	\	\	\	294	-118	79%	2.19	
	17,508	200	-96	-301	-152	304	99	56	56	56	107	1	205	-103	76%	1.91	
	18,007	200	-40	-194	-153	303	100	\	\	\	\	\	303	-100	75%	2.64	
	19,509	200	-69	-253	-183	287	98	41	27	34	94	2	190	-135	84%	1.46	
	200-300	18,006	210	-33	-234	-150	305	97	181	61	128	150	3	228	-103	76%	1.75
		18,013	210	-91	-200	-135	313	100	\	\	\	\	\	313	-101	75%	1.14
18,005		230	-8	-223	-136	313	86	296	5	161	170	14	241	-85	71%	4.29	
19,003		230	-18	-223	-152	304	100	\	\	\	\	\	304	-103	76%	4.02	
17,014		230	-69	-244	-170	294	100	\	\	\	\	\	294	-111	78%	1.77	
17,005		235	-25	-237	-159	299	100	\	\	\	\	\	299	-108	77%	1.72	
18,011		245	-98	-290	-191	282	100	\	\	\	\	\	282	-124	81%	3.75	
19,005		250	-97	-226	-157	301	100	\	\	\	\	\	301	-101	75%	2.63	
18,502		260	-51	-281	-164	297	100	\	\	\	\	\	297	-121	80%	4.46	
17,504		275	-119	-282	-191	282	100	\	\	\	\	\	282	-134	83%	1.73	
14,005		280	-13	-291	-183	287	93	188	74	119	145	7	216	-131	83%	<1	
18,010		280	-168	-306	-238	256	100	\	\	\	\	\	256	-188	97%	3.00	
18,003		300	-37	-177	-115	324	97	119	11	73	117	3	221	-97	74%	3.32	
> 300	17,502	320	-120	-284	-194	281	100	\	\	\	\	\	281	-142	85%	2.10	
	17,001	345	-33	-285	-192	282	94	264	9	99	133	6	207	-141	85%	5.08	
	17,006	410	-139	-263	-191	282	100	\	\	\	\	\	282	-134	83%	3.36	
	TC1675	420	-97	-241	-178	290	100	\	\	\	\	\	290	-119	80%	<1	

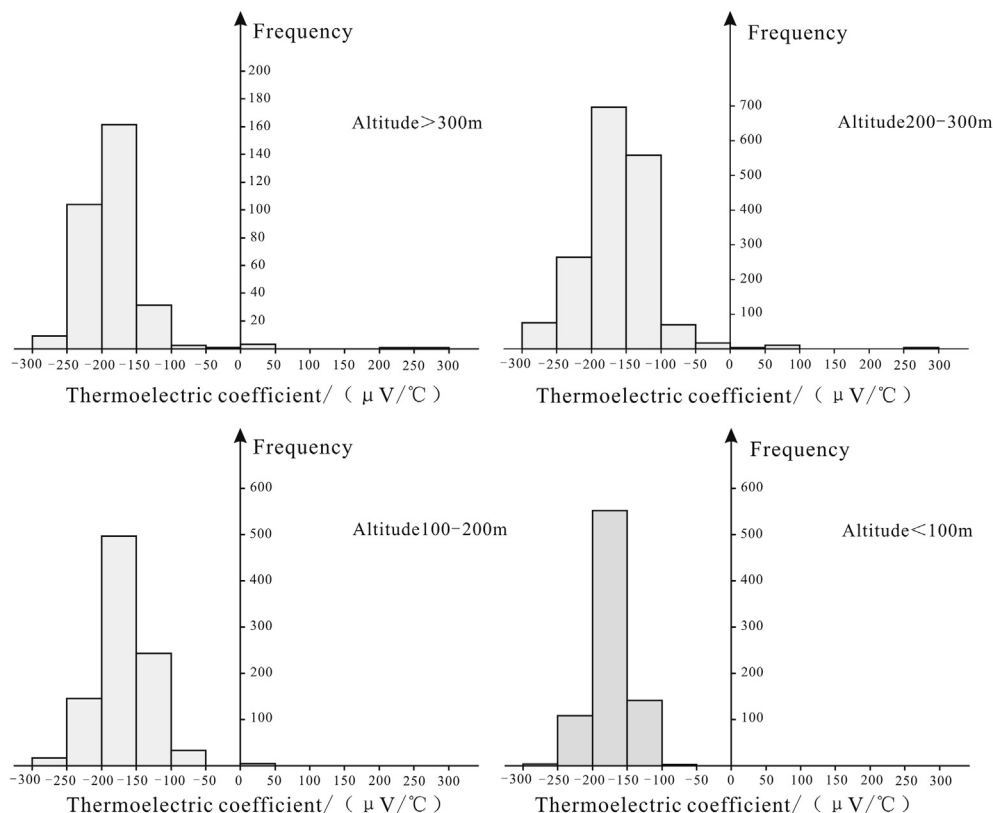


Fig 5. Histogram of pyrite thermoelectric coefficient distribution in ore bodies at different depths.

can be calculated by the values of Xnp, which is $\gamma = 50\text{-Xnp}/4$ (Yang and Zhang, 1991; Yang and Meng, 1991; Xue et al., 2014; Alam et al., 2019).

In the Yongxin gold deposit, the values of Xnp of pyrite range from -188 to -85 (Table 1) and the γ values range from 97% to 71% with an average of 79.4%. The Xnp and γ values of < 100 m level vary from -120 to -107 and 80% to 76%, with an average of -113.5 and 78.0% respectively. From 100 m to 200 m level, the values of Xnp range from -140 to -99 , with a mean of -116.2 , and the corresponding values of γ range from 85% to 75% with a mean of 79.0%. The values of Xnp and γ of 200–300 m level are -188 to -85 and 97% to 71%, with an average of -115.9 and 78.9%, respectively. The Xnp values of > 300 m level range from -142 to -119 , with an average of -134.0 , showing the corresponding γ values from 85% to 80%, with a mean value of 83.2% (Table 1).

5.1.3. Temperature estimation using pyrite thermoelectricity

Generally, the ore-forming temperatures can be determined by the values of pyrite thermoelectricity and conduction types. The N-type pyrite mostly forms at relatively high temperature conditions, whereas, most P-type pyrite occurs in low temperature environments. This is also supported by the observation that P-type pyrite grains tend occurring at shallower levels whereas N-type pyrite is precipitated at deeper levels (Chen et al., 1989). Therefore, the relationships between thermoelectricity and temperature can be defined by equations: (Zhang, 2010; Xue et al., 2014):

$$T(^{\circ}\text{C})_{\text{N-type}} = (704.51 - |\alpha|)/1.818$$

$$T(^{\circ}\text{C})_{\text{P-type}} = 3(122.22 + \alpha)/5.0$$

The measured pyrite thermoelectric coefficients from the Yongxin gold deposit when used in the above equations show that the average crystallization temperature of pyrite was 268°C , with the N-type pyrite grains crystallizing in the temperature range of $256\text{--}324^{\circ}\text{C}$ and P-type pyrite in the temperature range of $94\text{--}245^{\circ}\text{C}$ (Fig. 6). The crystallization temperatures of different pyrite types are concentrated mostly at 150°C (P-type pyrite) and 300°C (N-type pyrite). This range of temperature is consistent with the homogenization temperatures ($120\text{--}344^{\circ}\text{C}$) based on our fluid inclusion data (Table 1).

5.2. Fluid inclusion

5.2.1. Fluid inclusion petrography

Fluid inclusions in the Yongxin gold deposit are relatively small, occurring as oval, triangle, rectangle and irregular shapes, ranging from $1\ \mu\text{m}$ to $5\ \mu\text{m}$ in size in quartz and calcite. Based on phase changes during microthermometry experiments, the fluid inclusions in the Yongxin gold deposit can be divided into 3 types i.e. WL type (liquid + vapor but liquid-rich), WG type (liquid + vapor, but gas-rich) and G type (pure gas inclusions) (Fig. 7).

WL type inclusions: This type of inclusions often occur as irregular or oval shapes, with diameters of $3\text{--}10\ \mu\text{m}$ and contain bubbles

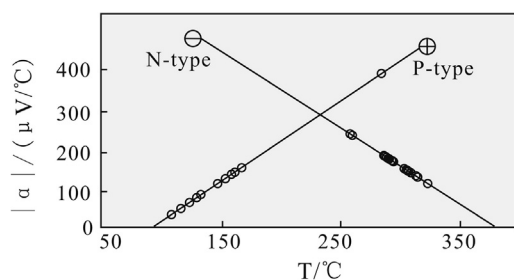


Fig. 6. Temperature estimation using pyrite thermoelectricity in the Yongxin gold deposit.

typically accounting for 1–25% of the total volume. Inclusions of WL type account for $> 50\%$ of the total number of inclusions and show isolated distribution in quartz. They always homogenize to vapor phase when heated.

WG type inclusions: This type of inclusions is rarer than WL type and accounts for approximately 10% of the total inclusions. They display rounded or oval shapes with diameters $< 10\ \mu\text{m}$ and contain bubbles typically accounting for 40% of the total volume. They always homogenize to vapor phase when heated.

G type inclusions: At room temperature, this type of inclusion displays bright color in the center and is black in the edges. They often occur as sub-rounded or oval shapes, with the size of $1\text{--}5\ \mu\text{m}$. This type of inclusions accounts for approximately 10% of the total number of inclusions.

5.2.2. Microthermometry

The microthermometric results, calculated salinities and densities (based on the $\text{H}_2\text{O}\text{-NaCl}$ system) are shown in Table 2 and Fig. 8. The fluid inclusions from the early ore forming stage (pyrite-quartz stage) to late ore forming stage (carbonate stage) are summarized and discussed below.

Fluid inclusions in pyrite-quartz stage (WL and WG type in quartz): The final ice melting temperatures of fluid inclusions range from -6.5°C to -1.5°C , corresponding to salinities of 2.5–10 wt% NaCl eqv. The homogenization temperatures are between 195°C and 355°C , with an average of 277°C . The fluid densities vary from 0.6 to $0.85\ \text{g}/\text{cm}^3$.

Fluid inclusions in pyrite stage (WL and WG type in quartz): The final ice melting temperatures of fluid inclusions in this stage range from -4.1°C to -0.9°C , corresponding to salinities of 1.5–7.0 wt% NaCl eqv. The homogenization temperatures are between 170°C and 310°C , with an average of 254°C . The fluid densities vary from 0.75 to $0.9\ \text{g}/\text{cm}^3$.

Fluid inclusions in gold-telluride-pyrite-galena-sphalerite stage (WL and WG type in quartz): The final ice melting temperatures of fluid inclusions range from -3.9°C to -0.2°C , corresponding to salinities of 0–6.0 wt.%NaCl eqv. The homogenization temperatures are between 120°C and 320°C with an average of 198°C . The fluid densities vary from 0.85 to $1.0\ \text{g}/\text{cm}^3$.

Fluid inclusions in carbonate stage (WL and WG type in calcite): The final ice melting temperatures of the fluid inclusions range from -3.6°C to -0.2°C , corresponding to salinities of 0.5–2.0 wt% NaCl eqv. The homogenization temperatures are between 120°C and 210°C , with an average of 165°C . The fluid densities vary from 0.9 to $1.0\ \text{g}/\text{cm}^3$.

5.2.3. Hydrogen-oxygen isotopes

The analytical results for oxygen and hydrogen isotopes of 7 quartz samples belonging to different ore-forming stages from the Yongxin gold deposit are shown in Table 3. Two samples belong to the pyrite-quartz stage and three samples are from the pyrite stage whereas the other two belong to the gold-telluride-pyrite-galena-sphalerite stage. The δD values range from -121.4‰ to -113.9‰ . The $\delta^{18}\text{O}_{\text{quartz}}$ values range from 0.6‰ to 9.7‰ and the $\delta^{18}\text{O}_{\text{water}}$ values range from -10.5‰ to -0.2‰ . All the plots of the O–H isotope values of the samples belonging to different ore forming stages straddle between meteoric water line and the magmatic water field, and closer to the meteoric water line in the $\delta^{18}\text{O}_{\text{water}}\text{-}\delta\text{D}$ diagram proposed by Sheppard (1977) (Fig. 9).

5.3. Rb-Sr isotope

The results of Rb–Sr dating from the Yongxin gold deposit are listed in Table 4. The concentrations of Rb and Sr range from 0.2037 to $5.982\ \mu\text{g}/\text{g}$ and 2.195 to $113.4\ \mu\text{g}/\text{g}$ respectively, with $^{87}\text{Rb}/^{86}\text{Sr}$ ratios of 0.0734–6.905 and corresponding $^{87}\text{Sr}/^{86}\text{Sr}$ ratios of

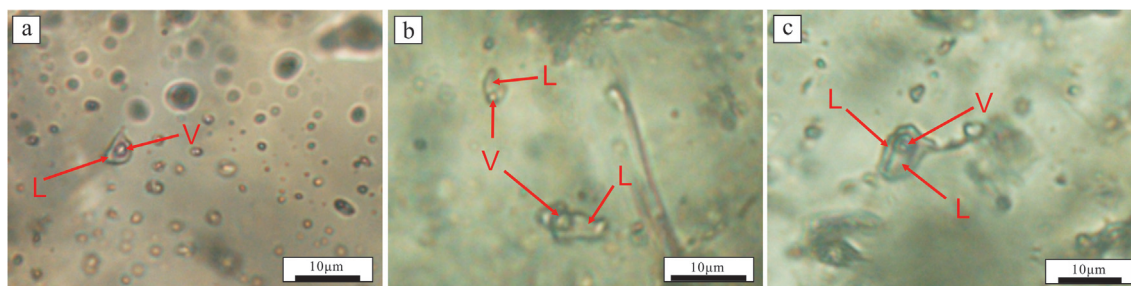


Fig 7. Photomicrographs of representative fluid inclusions in the Yongxin gold deposit.

Table 2

Microthermometry data of the fluid inclusions from the Yongxin gold deposit.

Ore-forming stage	Inclusion type	Size (μm)	Number	$T_{m. \text{ice}}$ ($^{\circ}\text{C}$)	T_h ($^{\circ}\text{C}$)	Salinity (% NaCl eqv.)	Density (g/cm^3)
Pyrite-quartz stage	WL + WG	3–10 μm	29	–6.5 to 1.5	270–290	2.5–10	0.6–0.85
Pyrite stage	WL + WG	2–5 μm	21	–4.1 to 0.09	230–270	1.5–7.0	0.75–0.9
gold-telluride-pyrite-galena-sphalerite stage	WL + WG + G + S	2–4 μm	44	–3.9 to 0.2	180–220	0.0–6.0	0.85–1.0
Carbonate stage	WL + WG + G	2–4 μm	9	–3.6 to 0.2	150–180	0.5–2.0	0.9–1.0

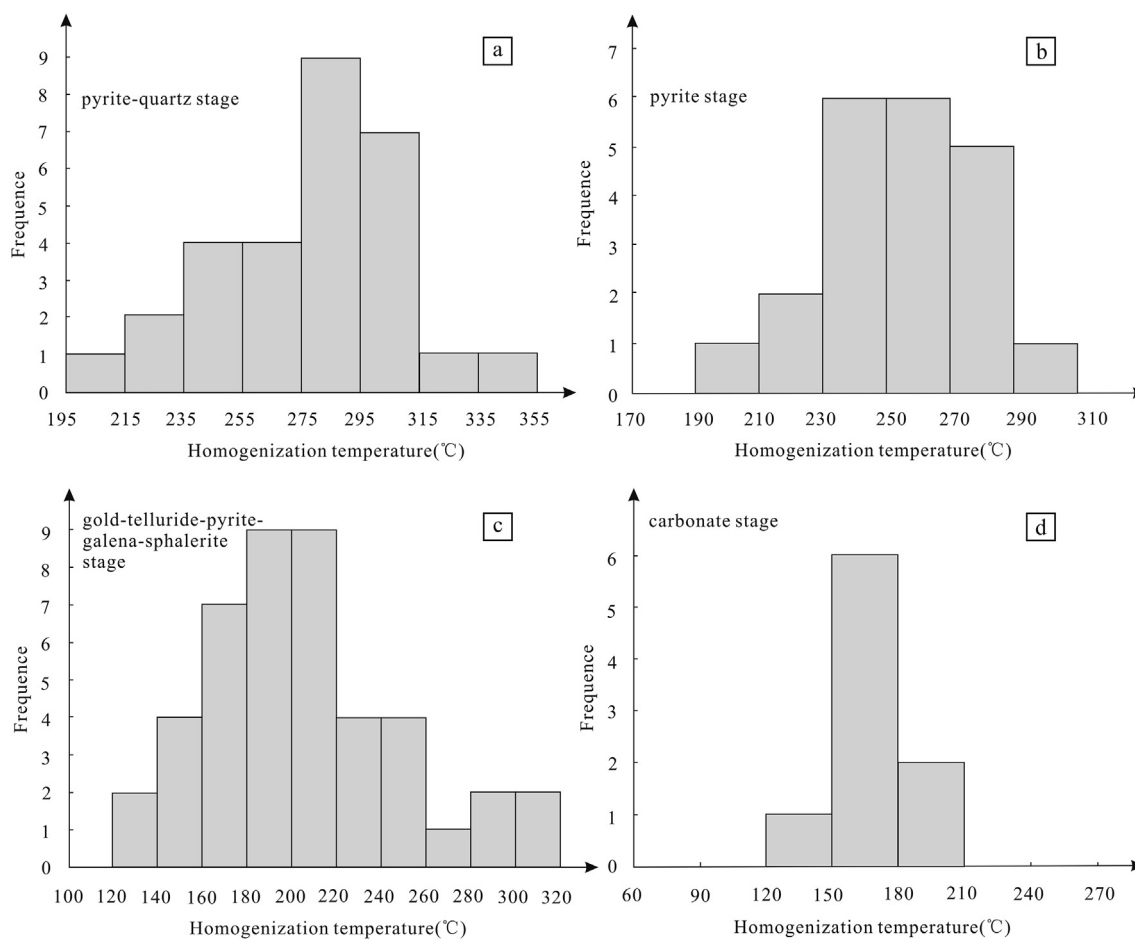


Fig 8. Histograms of homogenization temperatures of fluid inclusions in the Yongxin gold deposit.

0.710782–0.721897. The 8 samples analysed in this study (6 pyrites, one quartz and one calcite) display a strong linear array (Fig. 10) and yield a Rb-Sr isochron age of 114.6 ± 1.2 Ma (MSWD = 1.4) with an initial $^{87}\text{Sr}/^{86}\text{Sr}$ ratio of 0.710654 ± 0.000054 . 6 pyrites, one quartz and one calcite are from the same mineralization period, but different stages (Table 4).

5.4. Mineralogical mapping

Mineralogical mapping is one of the important advancements in modern mineralogical methods for ore prospecting (Yushkin, 1982). This method uses a variety of mineralogical parameters to qualitatively and quantitatively localize and orient mineralogical changes in various scales (profile, histogram, plane and three-dimensional map) to

Table 3
H-O isotopic compositions of the quartz veins from the Yongxin gold deposit.

Sample no.	Ore-forming stage	Mineral	δD	$\delta^{18}O_{\text{quartz}}$	$\delta^{18}O_{\text{water}}$
1	Pyrite-quartz stage	Quartz	-114.9	8.4	-1.5 to
2	Pyrite-quartz stage	Quartz	-117.6	9.7	0.2‰
3	Pyrite stage	Quartz	-118.9	0.6	-10.5 to
4	Pyrite stage	Quartz	-113.9	4.4	-6.7‰
5	Pyrite stage	Quartz	-121.3	7.8	
6	Gold-telluride-pyrite-galena-sphalerite stage	Quartz	-121.4	6.8	-9.5 to -7.0‰
7	Gold-telluride-pyrite-galena-sphalerite stage	Quartz	-119.3	5.3	

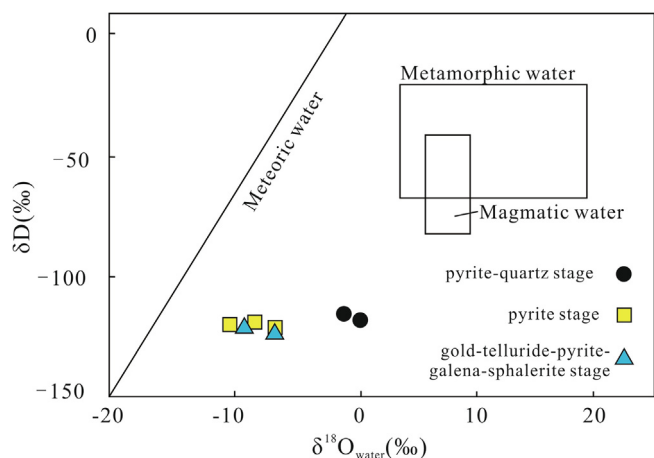


Fig 9. δD versus $\delta^{18}O_{H_2O}$ of the Yongxin gold deposit (modified after Sheppard, 1977).

understand the spatio-temporal distribution (Chen et al., 1988, 1989, 1996; Chen and Sun, 1990). As an important part of mineral typomorphism, the thermoelectricity characteristics of pyrite are sensitive enough to reflect mineral composition and crystal structure and are therefore a useful parameter for mineralogical mapping (Shao, 1988; Shao et al., 1990; Pang et al., 2012; Liu et al., 2013b; Xue et al., 2014; Li et al., 2016; Wang et al., 2019).

Here, the temperature, (percentage of P-type pyrite) P% and Xnp of pyrite were selected to perform mineralogical mapping. The mineralogical maps are horizontal projections, which are consistent with the geological maps (Fig. 2a). The sample distribution in our study covers the whole mining area and is evenly distributed from southeast to northwest of the deposit. The various parameters such as temperature, P% and Xnp of pyrite can be projected into a plane, which can be used for exploration and prediction of mineral deposits.

In general, the temperature of the ore-forming fluid decreases gradually with the migration away from the source, i.e. the closer to the source the higher metallogenic temperature. Therefore, the horizontal mapping of metallogenic temperature can help to track the source and

Table 4
Rb-Sr isotopic compositions of the pyrite, quartz and calcite from the Yongxin gold deposit.

No.	Sample name	Mineral	Rb ($\mu\text{g/g}$)	Sr ($\mu\text{g/g}$)	$^{87}\text{Rb}/^{86}\text{Sr}$	$^{87}\text{Sr}/^{86}\text{Sr}$	Altitude/m
1	D17014	Pyrite	5.982	2.558	6.905	0.721897 ± 7	210
2	D20506	Pyrite	3.674	3.962	2.739	0.715004 ± 9	120
3	D16504	Quartz	0.2037	2.459	0.2408	0.711024 ± 8	320
4	D18015	Pyrite	3.135	2.195	4.216	0.717568 ± 8	154
5	D17001-3	Pyrite	1.218	14.95	0.7459	0.711936 ± 9	345
6	D18003-3	Pyrite	3.408	3.751	2.673	0.715053 ± 7	295
7	D18005-5	Pyrite	2.961	6.824	1.281	0.712711 ± 9	225
8	D18029	Calcite	2.807	113.4	0.0734	0.710782 ± 9	250

flow direction of metallogenic fluid and reveal its evolution and migration path. In Fig. 11a. The temperature in the deep northwestern part of the deposit is obviously higher than that in the shallower southeastern domain.

P-type pyrite is more capable to carry Au than N-type. Different P-type pyrite percentages indicate different prospecting potential for the gold, and different isolines of P-type pyrite percentages indicate different ore-prospecting zones of gold deposits. Low, medium and high isolines correspond to low, medium and high-grade ores. Extraordinary high-grade ore is expected to occur when the percentage of the P-type pyrite is 100%. In the Yongxin gold deposit, the percentage of the P-type pyrite mainly ranges from 0% to 14% and displays obvious zonation on the horizontal plane. In Fig. 11b, there are 6 obvious high value regions, with the percentage of P-type pyrite higher than 1.5%. The six high value regions indicate 6 ore prospective areas marked A-F, which are distributed from the surface levels in the SE to the deeper levels in the NW, and these areas are considered as metallogenic prospective zones. In addition, previous studies have shown that the thermoelectric parameter (Xnp) of pyrite can, to some extent, indicate the potential of ore mineralization. The more positive thermoelectric parameters of pyrite are, the higher metallogenic potential is. Therefore, the positive thermoelectric parameter combined with the seven high value regions (i.e. 1-7) on the horizontal map (Fig. 11c) indicate the greater prospecting potential around ZK180-5 and ZK180-6 i.e. area B or 4 and C or 5 in Fig. 11b and c.

In order to verify the prediction of the prospecting, we carried out planar mapping of the average gold grade from different drilled cores in the Yongxin gold deposit (Fig. 11d). The map indicates eight high gold grade areas, marked as a-h. These eight locations are rich in gold, with > 4.8 g/t Au in the orebodies. The predicted metallogenic prospective areas i.e. ZK180-5 and ZK180-6 reliably present high Au grade mineralization.

6. Discussion

6.1. Mineralization age

Direct dating of the ore forming minerals from gold and other ore deposits has been carried out using multiple techniques. Among these, Rb-Sr isotopic dating of pyrite has been proved to be a robust method to determine the timing of ore mineralization (Yang and Zhou, 2001; Wang et al., 2014; Tian et al., 2019; Gao et al., 2020). Previous studies suggest that Rb-Sr isochron dating of the simultaneously formed hydrothermal mineral assemblages is more significant than that of a single mineral phase (e.g. Liu et al., 1998; Hu et al., 2015; Han et al., 2020). Li et al. (2008) carried out Rb-Sr dating on pyrite, sericite and quartz from the ore bodies in the Linglong gold deposit, and found that the Rb-Sr isochron ages of pyrite (120.4 ± 6.7 Ma), sericite (119.9 ± 1.3 Ma) and quartz (121.4 ± 2.4 Ma) were almost consistent, indicating that the minerals formed in the whole metallogenic process of the gold deposit were crystallized at the same time or the isotopes achieved equilibrium phase. In addition, Huang et al. (2016) selected sphaerite, galena, chalcocopyrite and quartz samples from the Jinchanghe Cu-Pb-Zn

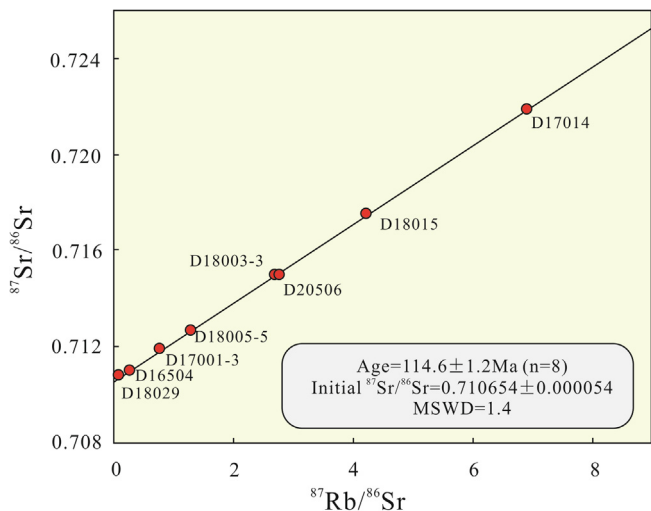


Fig 10. Rb-Sr isochron from pyrite, quartz and calcite in the Yongxin gold deposit.

deposit to carry out Rb-Sr dating which also gave consistent ages for different minerals such as sphalerite (118.9 ± 5.9 Ma), sphalerite + chalcopyrite (120.3 ± 5.1 Ma), sphalerite + galena + quartz (118.7 ± 1.5 Ma) and sphalerite + galena + chalcopyrite + quartz (118.9 ± 1.4 Ma). In addition, based on the work on the Luotuoshan polymetallic deposit by Yang et al. (2016), the Rb-Sr isochron ages of different minerals are also consistent i.e. galena gives an isochron age of 138.4 ± 7.6 Ma while that of pyrite and sphalerite + pyrite + galena was reported as 137.2 ± 3.7 Ma and 137.3 ± 2.6 Ma, respectively, which indicate that the Rb-Sr dating technique on hydrothermal mineral assemblages even from different ore-forming stages, is more reliable and accurate.

Our Rb-Sr isotopic data of pyrite, quartz and calcite assemblages reliably constrain the timing of ore formation of the Yongxin gold deposit, as it represents a closed system with homogeneous initial isotopic ratios and variably high Rb/Sr values. Our microscopic observations eliminate the existence of inclusions of sericite and feldspar in the

pyrite. Most of our samples yield reliable Rb and Sr isotopic composition, and therefore, we argue that the Rb-Sr isochron age of the pyrite reported in our study is reliable, and accurately constrain the timing of the major gold mineralization stage at 114.6 ± 1.2 Ma. The Au mineralization age was consistent with the emplacement timing of the diorite and granite porphyries (114.8 ± 1.9 Ma and 114.5 ± 1.5 Ma) (Li et al., 2017a). In addition, the age of the unaltered microdiorite, cutting the ore, is 109.9 ± 1.8 Ma (Li, 2018). All these arguments support that our Rb-Sr isochron age of the pyrite, quartz and calcite precisely constrains the metallogenic age of the Yongxin gold deposit. The Sandaowanzi Au, Shangmachang Au and Beidagou Au deposits, representing typical epithermal gold deposits in this tectonic belt, were formed in 115–125 Ma (Liu et al., 2013), 113.6 Ma (Gao et al., 2018) and 115.5 Ma (Gao et al., 2018) respectively. In summary, the early Cretaceous is the metallogenic concentration stage of gold deposits in the Duobaoshan belt. Based on the comprehensive information related to the petrogenesis and tectonic background of magmatic rocks closely related to the mineralization age (Li, 2018), it is believed that a series of gold deposits were formed due to the subduction of the Pacific Plate in the early Cretaceous.

6.2. Source and evolution of ore-forming fluids

The ore-forming fluid of the pyrite-quartz stage (first ore-forming stage) in the Yongxin gold deposit is represented by pure white quartz veins hosting fluid inclusions belonging to the H₂O-NaCl system, with moderate homogenization temperatures, low-medium salinity and low density. Subsequently, the ore-forming fluid evolved to H₂O-NaCl system characterized by low homogenization temperatures, low-medium salinity and low-medium density with abundant pyrite, belonging to the pyrite stage, represented by pyrite-quartz veins. Then, the ore-forming fluid migrated to shallow levels, leading to an inflow of meteoric-water that mixed with the hydrothermal fluid system. The ore-forming fluid evolved to the gold-telluride-pyrite-galena-sphalerite stage showing low homogenization temperatures, low salinity, and low-medium density. The late ore-forming fluid shows low homogenization temperatures, low-medium salinity and low-medium density, corresponding to the stage represented by carbonate minerals veins. The ore-forming fluid characteristics of the Yongxin gold deposit are similar

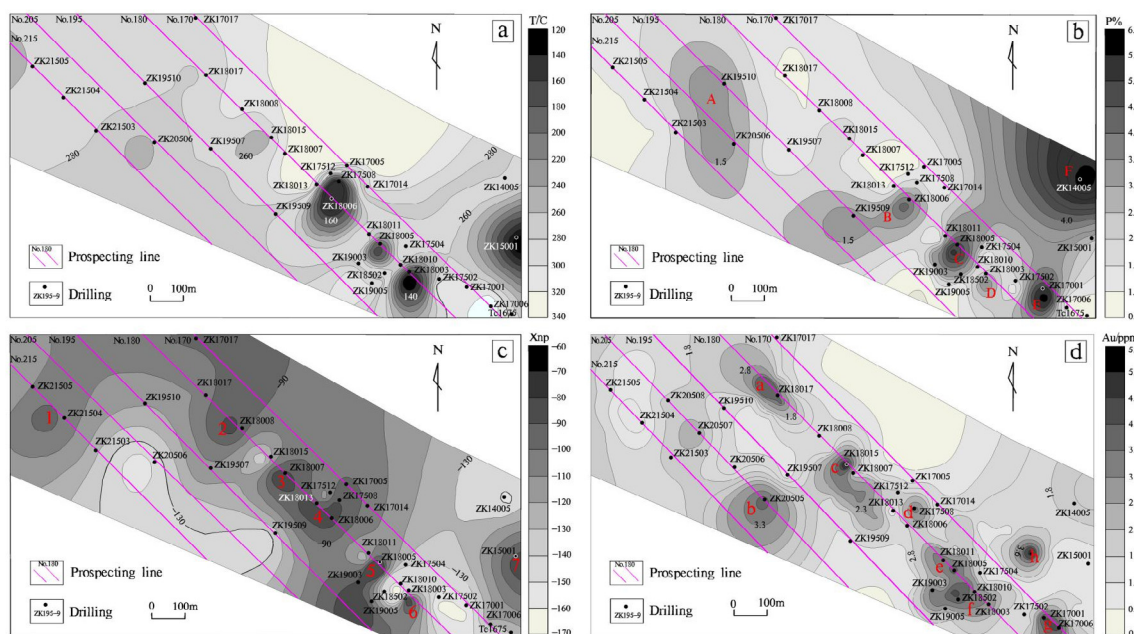


Fig 11. Horizontal mapping of different parameters of the Yongxin gold deposit: (a) Ore-forming temperature (estimated by pyrite thermoelectricity); (b) P-type percentage (estimated by pyrite thermoelectricity); (c) thermoelectric parameter (Xnp); (d) average gold grade of different drill cores.

with those of the gold deposits in the North China Craton (Li et al., 2014, 2015, 2017b, 2018b; Li and Santosh, 2014, 2017; Li et al., 2019b).

In summary, the quartz and pyrite of the early ore-forming stage were precipitated as the fluid cooled to ~ 355 °C to ~ 310 °C with the enrichment of the metallic minerals such as chalcopyrite, galena, sphalerite etc. The natural gold and telluride including calaverite, hessite, petzite and altaite crystallized mainly at about 120–320 °C. Finally, carbonate and clay minerals precipitated as the fluid cooled to 120 °C. The NE and NW-trending faults controlled the distribution of lithostratigraphic units and ore-bodies of the Yongxin gold deposit. The ore-forming fluids originated at depth in the NW part of the Yongxin gold deposit, and upwelled through structural locales to form ore-bodies, as revealed in the mineralogical map shown in Fig. 11a. The ore-forming temperature in the northwestern part of the deposit is obviously higher than that in the southeastern part of the deposit, indicating that the fluid gradually evolved from the deeper part in the northwest to the shallower part in the southeast (Fig. 11a).

The δD values of the Yongxin gold deposit show a narrow range, varying from -114.9‰ to -121.4‰ , and the $\delta^{18}\text{O}_{\text{water}}$ values range from -10.5‰ to -0.2‰ , with an average of -5.83‰ . All of these values lie between the magmatic water field and meteoric water line, but are slightly close to the meteoric water line in the $\delta^{18}\text{O}_{\text{water}}-\delta D$ diagram, which suggest a slight shift in isotopic composition of the fluid from early pyrite-quartz stage to later pyrite stage and Au-Te-sulfide which might be occurred due to the mixing of meteoric water.

6.3. Ore genesis and prospecting

The values of Xnp of pyrite range from -188 to -85 and the γ values range from 97% to 71% with an average of 79.4%. We conclude that the existing ore-body of the Yongxin gold deposit is basically the lower part of the ore-body, i.e. about 79.4% of ore-body has already been eroded. Thermoelectricity of pyrite of the Yongxin gold deposit is distributed in vertical zones in the axial direction. The value of Xnp and thermoelectricity of pyrite does not change significantly in the vertical direction, suggesting that the ore body extends further. Combined with the pyrite thermoelectric coefficients in different altitudes, we consider that there is still good potential in the deeper part of the deposit if N-P type pyrite continues to exist.

The Rb-Sr dating of the pyrite, quartz and calcite show that the deposit was formed during the early Cretaceous (114.6 ± 1.2 Ma). The magmatism and ore-forming processes were related to the subduction of the Paleo Pacific Plate (Li et al., 2017a). The NW-trending faults formed during the subduction, and provided the pathways and locales for Au-bearing fluid migration and precipitation (Yuan et al., 2018). The intersecting diorite porphyrite veins and ore bodies in multiple stages suggest the close genetic relationship between them (Li et al., 2017a; Li, 2018). The mineralization was spatio-temporally related to diorite porphyrite veins, which is also supported by the geochemical analysis of rare earth and trace elements (Li, 2018). The fluid inclusion study shows that the mineralization of the Yongxin gold deposit proceeded under low temperature, low-medium salinity and low-medium density conditions, and the ore-forming fluids of the Yongxin gold deposit are of a mixed magmatic and meteoric origin, which was also supported by He-Ar-S-Pb isotopic analysis (Li, 2018; Yuan et al., 2018). The metals were mainly derived from the magma and possibly originated from the mantle (Yang and Santosh, 2019), with minor contribution from the lower crustal rocks. The mixing of the magmatic water and meteoric water mainly controlled the precipitation mechanism of the metals including Au (Li, 2018).

In summary, the ore-forming fluids in the Yongxin gold deposit (containing S, Fe, Mo, Au, Ag, As, Co, Ni and Te) migrated from the northwestern deeper levels to the southeastern shallower part along the early Cretaceous tectonic faults and fractures with shallow dips (Li, 2018; Yuan et al., 2018). The ore bodies are distributed in veins along

the NW trending fracture zone. Our study suggests good potential for ore prospecting in the deeper northwestern part of the deposit. In the Fig. 11b and c, the locations showing the elevated values of P-type pyrite combined with high values of the thermoelectric parameters in the northwestern part of the deposit also support our speculation. The superimposed halo analysis of ore-forming elements (Au, Ag, As, Sb, Te, Mo, Mn and Co) was carried out for 400 ore samples from the drills. The horizontal projection contour maps of the ore-forming elements display a strong abnormal inner band in the deeper northwestern part of the deposit, which again indicates great prospecting potential (Li et al., 2019a).

7. Conclusions

- 1) The Yongxin gold deposit formed at a shallow depth, with relatively low ore-forming temperatures ranging from 120 °C to 355 °C, low-medium salinity ranging from 0 wt% to 10 wt%, and low-medium density ranging from 0.6 g/cm³ to 1.0 g/cm³. The ore-forming fluids were mainly composed of magmatic water mixed with meteoric water. Fluid mixing dominantly governed the mechanism that triggered the precipitation and deposition of ore-forming materials.
- 2) The Rb-Sr isotopic composition of pyrite, quartz and calcite in the Yongxin gold deposit provides reliable constraints about the timing of ore formation, and we report isochron age of pyrite, quartz and calcite as 114.6 ± 1.2 Ma.
- 3) The ore-forming fluids gradually evolved from the deeper northwestern part to the shallower southeast of the Yongxin gold deposit. The pyrite thermoelectric coefficient characteristics in different altitudes, the conduction type of the carriers of pyrite (N type or P type), Xnp and γ values and the mineralogical mapping indicate great prospecting potential around ZK180-5, ZK180-6 and in the deeper northwestern part of the deposit.

Declaration of Competing Interest

The authors declare that they have no known competing financial interests or personal relationships that could have appeared to influence the work reported in this paper.

Acknowledgements

We thank Yongjie Zeng and Shisheng Li for their assistance in the field work. This study was funded by the National Natural Science Foundation of China (grant no. 41872038), Ministry of Science and Technology of China for the State Key Research and Development Plan (grant no. 2016YFC0600106), Heilongjiang Provincial Land and Resources Research Project (grant no. 201603) and the Fundamental Research Funds for the Central University (grant no. 2652017247).

References

- Abraitis, P.K., Patrick, R.A.D., Vaughan, D.J., 2004. Variations in the compositional textural and electrical properties of natural pyrite: a review. *Int. J. Miner. Process.* 74, 41–59.
- Alam, M., Li, S.R., Santosh, M., Shah, A., Yuan, M.W., Khan, H., Qureshi, J.A., Zeng, Y.J., 2019. Morphological, thermoelectrical, geochemical and isotopic anatomy of auriferous pyrite from the Bagrote Valley placer deposits North Pakistan: implications for ore genesis and gold exploration. *Ore Geol. Rev.* <https://doi.org/10.1016/j.oregeorev.2019.103008>.
- Chen, G.Y., 1996. The development of modern genetic mineralogy in China. In: Development of geosciences disciplines in China. Wang Hongzhen et al. (Ed.). Wuhan: China University of Geosciences Press, 93–98.
- Chen, G.Y., Shao, W., Sun, D.S., 1989. Genetic mineralogy and prospecting of Jiaodong gold deposit. Chongqing: Chongqing publishing house. pp. 1–452 (in Chinese with English abstract).
- Chen and Sun, D.S., 1990. Principles of mineral typomorphism-six essential natures. Abs.1, 15th IMA, Beijing, 14–15 (in Chinese with English abstract).
- Chen, G.Y., Sun, D.S., Yin, H.A., 1987. Genetic Mineralogy and Mineral Mineralogy. Chongqing Publishing Group, pp. 35–41 (in Chinese with English abstract).
- Chen, G.Y., Sun, D.S., Yin, H.A., 1988. Genetic mineralogy and prospecting (2nd edition).

- Chongqing: Chongqing publishing house.1-880 (in Chinese with English abstract).
- Deng, C.Z., Sun, D.Y., Li, G.H., Lu, S., Tang, Z.Y., Gou, J., Yang, Y.J., 2019. Early cretaceous volcanic rocks in the Great Xing'an Range: Late effect of a flat-slab subduction. *J. Geodyn.* 124, 38–51.
- Du, Q., Zhao, Y.M., Lu, B.G., Ma, D.Y., Li, P.L., Lü, J.K., Li, W.S., Ao, L.Z., Cui, G., 1988. The Duobaoshan Porphyry Copper Deposit. Geological Publishing House, Beijing. pp. 1-334 (in Chinese with English abstract).
- Gao, R.Z., Xue, C.J., Lü, X.B., Zhao, X.B., Yang, Y.S., Li, C.C., 2017a. Genesis of the zhengguang gold deposit in the duobaoshan ore field, heilongjiang province, NE China: constraints from geology, geochronology and S-Pb isotopic compositions. *Ore Geol. Rev.* 84, 202–217.
- Gao, R.Z., Xue, C.J., Chi, G.X., Dai, J.F., Dong, C., Zhao, X.B., Man, R.H., 2020. Genesis of the giant caixiashan Zn-Pb deposit in Eastern Tianshan, NW China: Constraints from geology, geochronology and S-Pb isotopic geochemistry. *Ore Geol. Rev.* 119, 103366.
- Gao, S., Xu, H., Zang, Y.Q., Yang, L.J., Yang, B., Wang, T., 2017b. Late Mesozoic magmatism and metallogeny in NE China: The Sandaowanzi-Beidagou example. *Int. Geol. Rev.* 59 (11), 1413–1438.
- Gao, S., Xu, H., Zang, Y.Q., Wang, T., 2018. Mineralogy, ore-forming fluids and geochronology of the Shangmachang and Beidagou gold deposits, Heilongjiang province, NE China. *J. Geochem. Explor.* 188, 137–155.
- Ge, W.C., Wu, F.Y., Zhou, C.Y., Zhang, J.H., 2007. Porphyry Cu-Mo deposits in the eastern Xing'an-Mongolian orogenic belt: mineralization ages and their geodynamic implications. *Chin. Sci. Bull.* 52, 3416–3427 (in Chinese with English Abstract).
- Han, J.L., Sun, J.G., Liu, Y., Zhang, X.T., He, Y.P., Yang, F., Chu, X.L., Wang, L.L., Wang, S., Zhang, X.W., Zhao, C.T., 2020. Genesis and age of the Toudaoliuhe breccia-type gold deposit in the Jiapigou mining district of Jilin Province, China: Constraints from fluid inclusions, H-O-S-Pb isotopes, and sulfide Rb-Sr dating. *Ore Geol. Rev.* 118, 103356.
- Hao, Y.J., Ren, Y.S., Duan, M.X., Tong, K.Y., Li, C., 2015. Metallogenic events and tectonic setting of the Duobaoshan ore field in Heilongjiang Province, NE China. *J. Asian Earth Sci.* 97, 442–458.
- Hu, Q.Q., Wang, Y.T., Mao, J.W., Wei, R., Liu, S.Y., Ye, D.J., Yuan, Q.H., Dou, P., 2015. Timing of the formation of the Changba-Lijiagou Pb-Zn ore deposit, Gansu Province, China: evidence from Rb-Sr isotopic dating of sulfides. *J. Asian Earth Sci.* 103, 350–359.
- Huang, H., Zhang, C.Q., Zhou, Y.M., Xie, H.F., Liu, B., Xie, Y.F., Dong, Y.T., Yang, C.H., Dong, W.W., 2016. Rb-Sr isochron age of Jinchanghe Fe-Cu-Pb-Zn polymetallic deposit in Yunnan Province and its geological significance. *Mineral Depos.* 33 (1), 123–136 (in Chinese with English abstract).
- Karpov, I.K., 1981. *Physicochemical Computer Modeling in Geochemistry [in Russian]*. Nauka, Novosibirsk.
- Large, R.R., Danyushevsky, L., Hollit, C., Maslennikov, V., Meffre, S., Gilbert, S., Bull, S., Scott, R., Emsbo, P., Thomas, H., Singh, B., Foster, J., 2009. Gold and trace element zonation in pyrite using a laser imaging technique: implications for the timing of gold in orogenic and Carlin-style sediment-hosted deposits. *Econ. Geol.* 104, 635–668.
- Lehner, S., Savage, K., Ciobanu, M., Cliffel, D.E., 2007. The effect of As, Co, and Ni impurities on pyrite oxidation kinetics: an electrochemical study of synthetic pyrite. *Geochim. Cosmochim. Acta* 71 (10), 2491–2509.
- Li, C.L., 2018. *Gold metallogeny and prospecting in the Nenjiang-Heihe tectonic melange zone, Heilongjiang*. PhD. Dissertation of China University of Geosciences Beijing (in Chinese with English abstract).
- Li, C.L., Li, S.R., Xu, W.X., Yuan, M.W., Li, S.S., Qu, H., Wang, Z., 2018a. Typomorphic characteristics and stable isotopes of pyrite from the Yongxin tellurium-gold deposit in Heilongjiang province. *Bull. Mineral. Petrol. Geochem.* 37 (1), 75–86 (in Chinese with English abstract).
- Li, C.L., Xu, W.X., Yu, Y.B., Li, G.H., Li, S.R., Yuan, M.W., Li, S.S., Xu, G.Z., 2017a. Geochronology and geochemistry of the ore-related magmatic rocks from the Yongxin gold deposit, Northwest Xiao Hinggan Mountains and their ore-forming tectonic implication. *Geoscience* 31 (6), 1114–1130 (in Chinese with English Abstract).
- Li, C.L., Li, S.R., Luo, J.Y., Song, J.Y., Zhang, J.Q., 2009. Thermoelectric coefficient, conductive type and significance of the pyrite from Yixingzhai gold deposit in Fanshi county, Shanxi Province, China. *Geoscience* 12 (3), 1056–1063 (in Chinese with English Abstract).
- Li, C.L., Yu, Y.B., Yuan, M.W., Li, S.R., Xu, W.X., Zhu, J., Li, S.S., 2019a. Discovery and geological significance of Gold-silver bearing minerals and tellurides in the Yongxin gold deposit, NE of Great Xing'an Range. *Earth Science Frontiers*. <https://doi.org/10.13745/j.esf.sf.2019.8.20> (in Chinese with English Abstract).
- Li, J., Shen, J.F., Cao, W.D., Peng, Z.D., Li, J.C., Liu, H.M., Wei, Z.J., Wang, J.X., Liu, S.Q., Wang, D.L., Wang, S.H., 2016. Thermoelectricity of pyrite and deep prospecting of the Gangcha gold deposit, Gansu Province, China. *Bull. Mineral. Petrol. Geochem.* 35 (2), 378–386 (in Chinese with English abstract).
- Li, L., Santosh, M., Li, S.R., 2015. The “Jiaodong type” gold deposits: Characteristics, origin and prospecting. *Ore Geol. Rev.* 65, 589–611.
- Li, L., Li, S.R., Santosh, M., Zhu, J., Suo, X.J., 2018b. Early Jurassic decretion gold metallogenesis in the Eastern North China Craton: Constraints from S-Pb-C-D-O isotopic systematics and pyrite Rb-Sr geochronology of the Guilaizhuang Te-Au deposit. *Ore Geol. Rev.* 92, 558–568.
- Li, L.Q., Chen, F.K., Yang, J.H., Fan, H.R., 2008. Single grain pyrite Rb-Sr dating of the Linglong gold deposit, eastern China. *Ore Geol. Rev.* 34, 263–270.
- Li, S.R., 1994. Thermoelectricity of pyrite from the Jinqingding gold deposit in the Jiaodong region. *Geol. Explor. Non-ferrous Metals* 3 (5), 302–307 (in Chinese with English abstract).
- Li, S.R., Santosh, M., Zhang, H.F., Luo, J.Y., Zhang, J.Q., Li, C.L., 2014. Metallogeny in response to lithospheric thinning and craton destruction: geochemistry and U-Pb zircon chronology of the Yixingzhai gold deposit, central north china craton. *Ore Geol. Rev.* 56 (1), 457–471.
- Li, S.R., Santosh, M., 2014. Metallogeny and craton destruction: records from the North China Craton. *Ore Geol. Rev.* 56, 376–414.
- Li, S.R., Santosh, M., 2017. Geodynamics of heterogeneous gold mineralization in the North China Craton and its relationship to lithospheric destruction. *Gondwana Res.* 50, 267–292.
- Li, S.S., Li, L., Li, S.R., Santosh, M., Yuan, M.W., Zhi, Z.Y., Wen, Z.H., 2019b. Physicochemical conditions governing the formation of gold deposits along the southern margin of the North China Craton: a case study from the Chen'er deposit. *Geol. J.* 1–19. <https://doi.org/10.1002/gj.3584>.
- Li, Y.J., Li, S.R., Santosh, M., Mo, X.X., Gao, K.B., Ma, Y., 2017b. Isotope geochemistry and geochronology of the Niujuan silver deposit, northern North China Craton: implications for magmatism and metallogeny in an extensional tectonic setting. *Ore Geol. Rev.* 90, 36–51.
- Liu, B., 2001. Density and isochoric formulae for NaCl-H₂O inclusions with medium and high salinity and their applications. *Geol. Rev.* 47, 617–622 (in Chinese with English abstract).
- Liu, B., Duan, G.X., 1987. NaCl-H₂O Density and isochoric formulae for NaCl-H₂O inclusions and their applications. *Acta Mineralogica Sin.* 7, 345–352 (in Chinese with English abstract).
- Liu, C.H., Liu, J.J., Wang, J.P., Wu, J., Wang, W.Y., Wang, L.X., Yu, K.W., Chen, D., Li, Z.G., 2013. Thermoelectric characteristics of pyrite from the main ore zone of the Huachangou gold deposit, Shaanxi Province and its significance. *Earth Sci. Front.* 20 (4), 264–272 (in Chinese with English abstract).
- Liu, H.N., Liu, J.J., Li, X.W., Liu, C.H., Dai, H.Z., Tao, Y.L., Wang, J.F., Du, Y.D., Fan, Y.F., 2018. Thermoelectric characteristics of pyrite from the Xindigou gold deposit in Inner Mongolia and its significance on deep prospecting. *Geol. China* 45 (4), 819–838 (in Chinese with English abstract).
- Liu, J., Li, Y., Zhou, Z.H., Ouyang, H.G., 2017. The Ordovician igneous rocks with high Sr/Y at the Tongshan porphyry copper deposit, satellite of the Duobaoshan deposit, and their metallogenic role. *Ore Geol. Rev.* 86, 600–614.
- Liu, J.L., Zhao, S.J., Cook, N.J., Bai, X.D., Zhang, Z.C., Zhao, Z.D., Zhao, H.B., Lu, J., 2013a. Bonanza-grade accumulations of gold tellurides in the Early Cretaceous Sandaowanzi deposit, northeast China. *Ore Geol. Rev.* 54 (8), 110–126.
- Liu, J.M., Zhan, S.R., Shen, J., Jiang, N., Huo, W.G., 1998. Review on direct isotopic dating of hydrothermal ore-forming processes. *Prog. Geophys.* 13, 46–55 (in Chinese with English abstract).
- Lu, H.Z., Fan, H.R., Ni, P., Ou, G.X., Shen, K., Zhang, W.H., 2004. *Fluid Inclusions*. Science Press, Beijing. PP. 1–444 (in Chinese with English abstract).
- Ludwig, K., 2003. *Isoplot 3.00: A Geochronological Toolkit for Microsoft Excel*. Berkeley: Berkeley Geochronology Center. 39.
- Ludwig, K., 2001. *Isoplot/Ex, version 2.49: a geochronological toolkit for Microsoft Excel*. Berkeley Geochronology Center. Special Publication. No1, 1–58.
- Miao, L.C., Fan, W.M., Zhang, F.Q., 2003. Chronology research of Xinkailin-Keluo complex in Lesser Hinggan Mountains. *Chin. Sci. Bull.* 48, 2315–2323 (in Chinese with English Abstract).
- Niu, S.D., Li, S.R., Santosh, M., Zhang, D.H., Li, Z.D., Shan, M.J., Lan, Y.X., Gao, D.R., Zhao, W.B., 2016. Mineralogical and isotopic studies of base metal sulfides from the Jiawula Ag-Pb-Zn deposit, Inner Mongolia, NE China. *J. Asian Earth Sci.* 115, 480–491.
- Pang, A.J., Li, S.R., Wang, X., Xing, J.R., 2012. A study on correlations of thermoelectric coefficient, thermal resistance rate of pyrite and golden mineralization in the Dujiaya gold deposit, East Shandong Province. *Bull. Mineral. Petrol. Geochem.* 31 (5), 495–504 (in Chinese with English abstract).
- Popova, 1974. The possibility and Perspektivy of the development of the thermotectonic motor of the study of ore minerals. ZMO. the entrance. pp.5 (in Russian).
- Roedder, E., 1984. Fluid inclusions. *Rev. Miner. Mineral. Soc. Am.* 12, 1–644.
- Pridmore, D.F., Shuey, R.T., 1976. The electrical resistivity of galena, pyrite, and chalcopyrite. *Am Mineral.* 61, 248–259.
- Savage, K.S., Stefan, D., Lehner, S.W., 2008. Impurities and heterogeneity in pyrite: influences on electrical properties and oxidation products. *Appl. Geochem.* 23 (2), 103–120.
- Schieck, R., Hartmann, A., Fiechter, S., Koenkamp, R., Wetzel, H., 1990. Electrical properties of natural and synthetic pyrite (FeS₂) crystals. *J. Mater. Res.* 5, 1567–1572.
- Seifullip, 1978. Thermoelectric properties of ore Minerals, herald of Leningrad. Univ. pp.6 (in Russian).
- Shao, W., Chen, G.Y., Sun, D.S., 1990. Method of investigating thermoelectricity of pyrite and its application to pyrites from gold deposits in Jiaodong region. *Geoscience* 4 (1), 45–56 (in Chinese with English Abstract).
- Shao, J., 1988. *Exploration Mineralogy of Gold Deposits (in Chinese)*. China University of Geosciences Press, Wuhan. pp. 38–45.
- Shen, J.F., Li, S.R., Ma, G.G., Liu, Y., Yu, H.J., Liu, H.M., 2013. Tyomorphic characteristics of pyrite from the Linglong gold deposit: its vertical variation and prospecting significance. *Earth Sci. Front.* 20 (3), 55–75 (in Chinese with English Abstract).
- Shepherd, T.J., Rankin A.H., Alderton D.H.M., 1985. *A Practical Guide to Fluid Inclusion Studies*. Chapman & Hall, Blackie. pp. 1–239.
- Sheppard, S.M.F., 1977. Identification of the origin of ore-forming solutions by the use of stable isotopes. *Geol. Soc., London, Special Publications.* 7, 25–41.
- Song, G.X., Cook, N.J., Wang, L., Qin, K.Z., Cristiana, L.C., Li, G.M., 2019. Gold behavior in intermediate sulfidation epithermal systems: a case study from the zhengguang gold deposit, heilongjiang province, NE-China. *Ore Geol. Rev.* 106, 446–462.
- Tian, Y.F., Ye, H.S., Mao, J.W., Wang, X.X., Jian, W., Wang, P., Ke, C.H., Zhang, X.K., 2019. Geochronology and geochemistry of the Dianfang gold deposit, western Henan Province, central China: Implications for mineral exploration. *Ore Geol. Rev.* 111,

- 102967.
- Wang, D.L., Shen, J.F., Qiu, H.C., Du, B.S., Li, J.P., Nie, X., Wang, Y.H., 2019. Study on typomorphic characteristics of pyrite and prediction of deep prospecting of Wulong gold deposit in Liaoning Province. *J. Nanjing Univers. (Nat. Sci.)* 55 (6), 898–915 (in Chinese with English abstract).
- Wang, G.W., Feng, Y., Carranza, E.J.M., Li, R.X., Li, Z.L., Feng, Z.K., Zhao, X.D., Wang, D.J., Kong, L., Jia, W.J., Wen, B.T., 2016. Typomorphic characteristics of pyrite: criteria for 3D exploration targeting in the Xishan gold deposit, China. *J. Geochem. Explor.* 164, 136–163.
- Wang, Y.B., Zeng, Q.D., Liu, J.M., 2014. Rb-Sr dating of gold-bearing pyrites from Wulaga gold deposit and its geological significance. *Resour. Geol.* 64 (3), 262–270.
- Wu, G., Chen, Y.C., Sun, F.Y., Liu, J., Wang, G.R., Xu, B., 2015. Geochronology, geochemistry, and Sr-Nd-Hf isotopes of the early Paleozoic igneous rocks in the Duobaoshan area, NE China, and their geological significance. *J. Asian Earth Sci.* 97, 229–250.
- Wu, J.C., Shen, J.F., Li, G.W., Li, S.R., He, Z.Y., Du, B.S., Xu, K.X., Qiu, H.C., Li, J.P., 2019. The improved method for measuring thermoelectric property of pyrite and its implication for exploring gold resources-A case study of the Wulong gold deposit in Liaoning Province. *Bulletin of Mineralogy, Petrology and Geochemistry*. <https://doi.org/10.19658/j.issn.1007-2802.2020.03.001> (in Chinese with English abstract).
- Xue, J.L., Li, S.R., Sun, W.Y., Zhang, Y.Q., Zhang, X., 2014. Characteristics of the genetic mineralogy of pyrite and its significance for prospecting in the Denggezhuang gold deposit, Jiaodong peninsula. *China. Sci. Chin. Earth Sci.* 57 (4), 644–661.
- Yang, C.X., Santosh, M., 2019. Ancient deep roots for Mesozoic world-class gold deposits in the north China craton: an integrated genetic perspective. *Geosci. Front.* <https://doi.org/10.1016/j.gsf.2019.03.002>.
- Yang, C.Y., Ye, H.S., Xiang, J.F., Chen, X.D., Xing, B., Li, L., Wang, S., 2016. Rb-Sr isochron age of sulfide minerals in Luotuoshan pyrite-polymetallic deposit of western Henan Province and its geological significance. *Mineral Depos.* 35 (3), 573–590 (in Chinese with English abstract).
- Yang, J.H., Zhou, X.H., 2001. Rb-Sr, Sm-Nd, and Pb Isotope systematics of pyrite: implications for the age and genesis of lode gold deposit. *Geology* 29 (8), 711–714.
- Yang, Z.S., Chen, G.Y., Sun, D.S., Wang, Z.J., 1999. Study on the hanging wall-rock alteration and typomorphic characteristics of pyrite in Cangshang gold deposit, northwestern Jiaodong. *Geoscience* 13 (1), 73–77 (in Chinese with English Abstract).
- Yang, G., Meng, W.P., 1991. The mechanism of pyrite thermoelectricity in the application of prospecting mineralogy of gold ore (in Chinese). *Proceedings of 3th National Conference of Placer Mineral, China*.
- Yang, G., Zhang, Y.H., 1991. The relationship between pyrite thermoelectricity and ore forming temperature and its significance in gold deposits (in Chinese). *Geol. Inf. Shandong.* 1, 20–25.
- Yang, Z.S., Li, H.Y., Gao, Z.M., Wang, Z.J., 2000. A study on thermoelectricity of pyrite from super high-grade gold deposits, northern Jiaodong. *Mineral Depos.* 19 (4), 307–314 (in Chinese with English Abstract).
- Yuan, M.W., Li, S.R., Li, C.L., Santosh, M., Masroor, A., Zeng, Y.J., 2018. Geochemical and isotopic composition of auriferous pyrite from the Yongxin gold deposit, Central Asian Orogenic Belt: Implication for ore genesis. *Ore Geol. Rev.* 93, 255–267.
- Yuan, M.W., Li, L., Li, S.R., Li, C.L., Santosh, M., Alam, M., Bao, X.B., 2019. Mineralogy, fluid inclusions and S-Pb-H-O isotopes of the Erdaokan Ag-Pb-Zn deposit, Duobaoshan metallogenic belt, NE China: Implications for ore genesis. *Ore Geol. Rev.* 113, 103074.
- Yuan, M.W., Zeng, Y.J., Li, C.L., Li, S.S., Li, S.R., 2017. Quantitative and positioning study on the hydrothermal alteration and mineralization relationship of the Yongxin gold deposit in the nenjiang-heihe mélange zone, Heilongjiang Province. *Geoscience* 31, 278–289 (in Chinese with English Abstract).
- Yushkin, N.P., 1982. *Topomineralogy*. Moscow: Nedra Publishing House. 1-228 (in Russian).
- Zeng, Q.D., Liu, J.M., Chu, S.X., Wang, Y.B., Sun, Y., Duan, X.X., 2014. Re-Os and U-Pb geochronology of the Duobaoshan porphyry Cu-Mo-(Au) deposit, northeast China, and its geological significance. *J. Asian Earth Sci.* 79, 895–909.
- Zhang, Y., 2010. Genetic mineralogy and deep prospects of Zhaodaoshan gold deposit in Muping, East Shandong Province. Master dissertation Chinese university of geosciences, Beijing. pp. 38-54 (in Chinese with English Abstract).
- Zhao, C., Qin, K.Z., Song, G.X., Li, G.M., Li, Z.Z., 2019a. Early Palaeozoic high-Mg basalt-andesite suite in the Duobaoshan porphyry Cu deposit, NE China: constraints on petrogenesis, mineralization, and tectonic setting. *Gondwana Res.* 71, 91–116.
- Zhao, Y.M., Zhang, D.Q., 1997. *Metallogeny and Prospective Evaluation of Copper-Polymetallic Deposits in the Great Hinggan Range and Its Adjacent Regions*. Seismological Press, Beijing. pp. 48-82 (in Chinese with English Abstract).
- Zhao, Z.H., Sun, J.G., Li, G.H., Xu, W.X., Lü, C.L., Guo, Y., Liu, J., Zhang, X., 2019b. Zircon U-Pb geochronology and Sr-Nd-Pb-Hf isotopic constraints on the timing and origin of the Early Cretaceous igneous rocks in the Yongxin gold deposit in the Lesser Xing'an Range NE China. *Geol. J.* 1–20.